The Astrophysical Journal, 738:57 (11pp), 2011 September 1 doi:10.1088/0004-637X/738/1/57

THE TEMPERATURE OF HOT GAS HALOS OF EARLY-TYPE GALAXIES

S. Pellegrini
Astronomy Department, University of Bologna, via Ranzani 1, I-40127 Bologna, Italy; silvia.pellegrini@unibo.it
Received 2011 March 22; accepted 2011 June 14; published 2011 August 11

ABSTRACT

Recently, the temperature T and the luminosity L_X of the hot gas halos of early-type galaxies have been derived, with unprecedented accuracy, from *Chandra* data for a sample of 30 galaxies, covering a wider range of galactic luminosity (and central velocity dispersion σ_c) than before. This work investigates the origin of the observed temperatures by examining the relationship between them and the galaxy structure, the gas heating due to Type Ia supernovae (SNe Ia) and the gravitational potential, and the dynamical status of the gas flow. In galaxies with $\sigma_c \lesssim 200$ km s^{-1}, the T's are close to a fiducial average temperature of gas in outflow; at $200 < \sigma_c$ (km s^{-1}) < 250, the T's are generally lower than this and unrelated to σ_c, which requires a more complex gas flow status; at larger σ_c, the T's may increase as σ_c^2, as expected for infall heating, though heating from SNe Ia, that is independent of σ_c, should be dominant. All observed T's are larger than the virial temperature, by up to ∼0.5 keV. The additional heating can be provided in the X-ray brightest galaxies by SNe Ia and infall heating, with an SN Ia energy input even lower than in standard assumptions; in the X-ray fainter ones it can be provided by SNe Ia, whose energy input would be required to be close to the full standard value at the largest σ_c. This same energy input, though, would produce temperatures larger than observed at low σ_c if entirely thermalized. The values of the observed T's increase from outflows to inflows; the gas is relatively hotter in outflows, however, if the T's are rescaled by the virial temperature. For $200 < \sigma_c$(km s^{-1}) < 250, lower L_X values tend to correspond to lower T's, a result that deserves further investigation.

Key words: galaxies: elliptical and lenticular, cD – galaxies: fundamental parameters – galaxies: ISM – galaxies: kinematics and dynamics – X-rays: galaxies – X-rays: ISM

Online-only material: color figures

1. INTRODUCTION

The advent of the *Chandra X-ray Observatory*, with its unprecedented subarcsecond resolution, allowed researchers to study better than ever before the main contributors to the total X-ray emission of early-type galaxies (hereafter ETGs): low-mass X-ray binaries (LMXBs; Fabbiano 2006), a population of weak sources such as late-type stellar coronae, cataclysmic variables, coronally active binaries (Pellegrini & Fabbiano 1994; Revnivtsev et al. 2008), the nuclear emission due to a supermassive black hole (MBH; e.g., Gallo et al. 2010; Pellegrini 2010), and a hot interstellar medium (ISM) with a temperature of a few million degrees. After careful subtraction of the stellar (resolved and unresolved) and nuclear emissions, the properties of the hot ISM could be characterized with unprecedented accuracy. Recently, this was done for a sample of 30 normal (non-cD) ETGs observed with *Chandra* to a depth that ensured the detection of bright LMXBs (Boroson et al. 2011, hereafter BKF). This is the first X-ray sample of ETGs covering a wide range of galactic luminosity, central velocity dispersion σ_c, and hot gas emission L_X; the X-ray properties of the hot gas (e.g., the luminosity L_X and the average temperature T) were derived in a homogeneous way, using a complete and accurate procedure to subtract all kinds of non-gaseous emissions (nucleus, detected and undetected LMXBs, and unresolved weak stellar sources). This approach resulted in a larger fraction of hot gas-poor galaxies than in previous samples, with L_X extending down to much lower values than before (∼10^{38} erg s^{-1}) and showing a variation of up to ∼ three orders of magnitude at the same galactic luminosity (see also David et al. 2006; Diehl & Statler 2007; Memola et al. 2009). Such a wide variation, even larger than found previously, had been linked to the origin and evolution of the hot ISM, and provided evidence for the effectiveness of an internal heating mechanism (e.g., from Type Ia supernovae, hereafter SNe Ia) to regulate gas evolution and produce very different content of the gas in ETGs in the present epoch (Loewenstein & Mathews 1987; David et al. 1990; Ciotti et al. 1991). The action of external agents (gas stripping, confinement, accretion) to reduce or enhance the hot gas content was also invoked (e.g., White & Sarazin 1991; Brown & Bregman 2000; Sun et al. 2007).

With this new characterization of the hot gas, BKF revisited the relationships between fundamental properties of the hot gas and those of the host galaxy, such as the $L_X - T$, $L_X - \sigma_c$, and $T - \sigma_c$ relations, where σ_c is a representative measure of the depth of the galactic potential well (Eskridge et al. 1995; O'Sullivan et al. 2001, 2003). L_X correlates positively with T and σ_c, though with a wide variation at fixed σ_c and T. Interestingly, the best-fit relation $L_X \propto T^{4.5}$, close to that already known for X-ray-luminous ETGs (O'Sullivan et al. 2003), is still moderately strong among ETGs with low T and L_X; also, in the $L_X - \sigma_c$ relation, ETGs with $kT > 0.4$ keV have the brightest X-rays (with one exception), while those with $kT < 0.3$ keV have the faintest X-rays. The least gas-rich ETGs are then the coolest ones, which seems contrary to the expectations that low L_X ETGs lose their ISM in an outflow (e.g., David et al. 1990; Ciotti et al. 1991) and that the hotter the gas, the stronger the outflow (BKF). On average, T increases with σ_c, and most ETGs lie above a rough estimate of the virial gas temperature ($T_\sigma = \mu m_p \sigma_c^2/k$), suggesting the presence of additional heating. ETGs with a moderate to high gas content ($L_X > 5 \times 10^{39}$ erg s^{-1}) follow a trend roughly parallel to that of T_σ; instead, ETGs with little hot gas ($L_X < 5 \times 10^{39}$ erg s^{-1}) have similar σ_c temperatures ranging from 160 to 250 km s^{-1}.

This lack of correlation was attributed to different dynamical states of the hot ISM in gas-poor and gas-rich ETGs, though a full explanation of this aspect remained to be found (BKF).

This work takes advantage of the new, accurate measurements of the hot gas properties and of the fundamental relations $L_X - \sigma_c$ and $T - \sigma_c$, derived down to galaxy masses and X-ray luminosities smaller than ever before (BKF), to investigate the relationships among T, galaxy structure, internal gas heating mechanisms (SNe Ia and those linked to the gravitational potential), and the dynamical status of the gas flow. A few characteristic temperatures are introduced that depend on the nature of the gas heating sources and galaxy structure, and are relevant for various gas-flow phases; these characteristic temperatures are then compared with the observed T values. In doing so, galaxy mass models are built according to the most recent understanding of the ETGs' structures, such as their stellar mass profile and dark matter content and distribution, as indicated by detailed modeling of optical observations and the main scaling laws (e.g., Cappellari et al. 2006; Weijmans et al. 2009; Auger et al. 2010; Napolitano et al. 2010; Shen & Gebhardt 2010). This paper aims to address the following questions: can the gas heating sources above account for the observed T's? How are the various input energy sources of the gas used in different flow phases? Is there any relation between T and the flow phase?

I present the sources of mass and heating for the hot ISM in Section 2, the conditions for the gas to escape from the galaxy in Section 3, the galaxy mass models in Section 4, the comparison between observed and predicted temperatures in Section 5, the relation between gas temperature and flow status in Section 6, and the conclusions in Section 7.

2. SOURCES OF MASS AND HEATING FOR THE HOT GAS

2.1. Gas Mass

In ETGs, the hot gas comes from stellar mass losses produced by evolved stars, mainly during the red giant, asymptotic giant branch, and planetary nebula phases, and by SNe Ia that are the only ones observed in an old stellar population (e.g., Cappellaro et al. 1999). The first, more quiescent, type of losses originates from ejecta that initially have the velocity of the parent star, then individually interact with the mass lost from other stars or with the hot ISM and mix with it (Mathews 1990; Parriott & Bregman 2008).

For a galaxy of total stellar mass M_*, the evolution of the stellar mass-loss rate $\dot{M}_*(t)$ can be calculated using single-burst stellar population synthesis models (Maraston 2005) for Salpeter and Kroupa initial mass functions (IMFs), assuming, for example, solar abundance. Doing so at an age of 12 Gyr, a rate of $\dot{M}_* = B \times 10^{-11}\, L_B(L_{B,\odot})\ M_\odot\ \mathrm{yr}^{-1}$ is recovered, where L_B is the galactic B-band luminosity at an age of 12 Gyr, and $B = 1.8$ or $B = 1.9$ for the Salpeter or Kroupa IMF (see also Pellegrini 2011). This value is in reasonable agreement with the average derived for nine local ETGs from *Infrared Space Observatory* data (Athey et al. 2002) of $\dot{M}_* = 7.8 \times 10^{-12}\ L_B(L_{B,\odot})\ M_\odot\ \mathrm{yr}^{-1}$, an estimate based on individual observed values that vary by a factor of $\sim$10 and were attributed to different ages and metallicities.

The total mass-loss rate of a stellar population $\dot{M}$ is given by the sum $\dot{M} = \dot{M}_* + \dot{M}_{\rm SN}$, where $\dot{M}_{\rm SN}$ is the rate of mass loss via SNe Ia events for the entire galaxy. $\dot{M}_{\rm SN}$ is given by $\dot{M}_{\rm SN} = M_{\rm SN}\, R_{\rm SN}$, where $M_{\rm SN} = 1.4\ M_\odot$ is the mass ejected by one event and $R_{\rm SN}$ is the explosion rate. $R_{\rm SN}$ has been determined to be $R_{\rm SN} = 0.16(H_0/70)^2 \times 10^{-12}\, L_B(L_{B,\odot})\,\mathrm{yr}^{-1}$ for local ETGs, where H_0 is the Hubble constant in units of km s^{-1} Mpc^{-1} (Cappellaro et al. 1999). More recent measurements of the observed rates of supernovae in the local universe (Li et al. 2011) give an SNe Ia rate in ETGs consistent with that of Cappellaro et al. (1999). For $H_0 = 70$ km s^{-1} Mpc^{-1}, one obtains $\dot{M}_{\rm SN} = 2.2 \times 10^{-13} L_B(L_{B,\odot})\ M_\odot\ \mathrm{yr}^{-1}$, which is $\sim$80 times smaller than the $\dot{M}_*$ derived above for an age of 12 Gyr; therefore, the main source of mass for the hot gas is provided by $\dot{M}_*$. A reasonable assumption is that the gas is shed by stars with a radial dependence that follows that of the stellar distribution, so that the density profile of the injected gas is $\rho_{\rm gas}(r) \propto \rho_*(r)$, where $\rho_*(r)$ is the stellar density profile. This assumption is adopted hereafter, and the characteristic temperatures presented below apply to a gas distribution following $\rho_{\rm gas}(r) \propto \rho_*(r)$ (but see also Section 5).

2.2. Heating from Stellar Motions and Supernovae

The material lost by stars is ejected at a velocity of a few tens of km s^{-1} and at a temperature of $\lesssim 10^4$ K (Parriott & Bregman 2008); it is subsequently heated to high, X-ray emitting temperatures by the thermalization of the stellar velocity dispersion as it collides with the mass lost from other stars or with ambient hot gas and is shocked. Another source of heating of stellar mass losses is provided by the thermalization of the kinetic energy of SNe Ia events. The internal energy given by these heating processes to the unit mass of injected gas is $3kT_{\rm inj}/2\mu m_p$ (where k is the Boltzmann constant, m_p is the proton mass, and μm_p is the mean particle mass, with $\mu = 0.62$ for solar abundance); $T_{\rm inj}$ is determined by the heating from thermalization of the motions of the gas-losing stars ($T_{\rm star}$) and of the velocity of the SNe Ia ejecta ($T_{\rm SN}$), and is written as (e.g., Gisler 1976; White & Chevalier 1983)

$$T_{\rm inj} = T_{\rm star} + T_{\rm SN} = \frac{\dot{M}_* T_* + \dot{M}_{\rm SN} T_{\rm ej}}{\dot{M}}. \quad (1)$$

Here, T_* is the equivalent temperature of the stellar motions (see below) and $T_{\rm ej} = 2\mu m_p E_{\rm SN}/(3kM_{\rm SN})$ is the equivalent temperature of the kinetic energy $E_{\rm SN}$ of the SNe Ia ejecta, with $E_{\rm SN} = 10^{51}$ erg for one event (e.g., Larson 1974). $T_{\rm ej}$ can be calculated by assuming that a factor f of $E_{\rm SN}$ is turned into heat; $f < 1$, since radiative energy losses from expanding supernova remnants may be important, and values down to $f = 0.1$ have been adopted (Larson 1974; Chevalier 1974). A value of $f = 0.85$ should not be too wrong for the hot, diluted ISM of ETGs (e.g., Tang & Wang 2005). In this way, $T_{\rm ej} = (f/0.85)1.5 \times 10^9$ K. By approximating $\dot{M} \simeq \dot{M}_*$ and using the estimates of Section 2.1 for $\dot{M}_{\rm SN}$ and $\dot{M}_*$ (for a Kroupa IMF) in the present epoch, one obtains $T_{\rm SN} \simeq 1.7(f/0.85) \times 10^7$ K.

The injection temperature $T_{\rm inj}$ is then the sum of two parts: one ($T_{\rm SN}$) is independent of the position within the galaxy where the gas is injected (i.e., independent of the radius in spherical symmetry) and is also constant from galaxy to galaxy (for a fixed IMF, age of the stellar population, and SNe Ia rate); however, for each ETG it can evolve with time if $\dot{M}_{\rm SN}$ and $\dot{M}_*$ evolve differently with time (Ciotti et al. 1991). The other part ($T_{\rm star}$) is basically independent of time but has a radial dependence and changes with galaxy structure, i.e., with the total mass and its distribution. An average T_* is obtained by calculating the mass-weighted gas temperature gained by the thermalization of the

stellar random motions $\langle T_* \rangle$:

$$\langle T_* \rangle = \frac{1}{k} \frac{\mu m_p}{M_*} \int 4\pi r^2 \rho_*(r) \sigma^2(r)\, dr, \quad (2)$$

where $\sigma(r)$ is the one-dimensional velocity dispersion of the stars. The integral term in Equation (2) is the same one that gives the kinetic energy associated with the stellar random motions [$E_{\rm kin} = 1.5 \int 4\pi r^2 \rho_*(r) \sigma^2(r)\, dr$] and enters the virial theorem for the stellar component; the mass-weighted temperature in Equation (2) is then often called "gas virial temperature." For a galaxy mass model made of stars and dark matter, characterized by $\mathcal{R} = M_h/M_*$, where M_h is the total dark mass and $\beta = r_h/r_*$, with r_h and r_* being the scale radii of the two mass distributions, $\langle T_* \rangle$ can be expressed using the central velocity dispersion σ_c as $\langle T_* \rangle = \mu m_p\, \sigma_c^2 \Omega(\mathcal{R}, \beta)/k$ (e.g., Ciotti & Pellegrini 1992). The function Ω increases slightly for larger $\mathcal{R}$ and for lower β, that is, for a larger amount of gravitating mass or a higher mass concentration, but Ω is always <1, since $\sigma(r)$ has in general a negative radial gradient (e.g., Section 4 and Figure 1). $\langle T_* \rangle$ is then proportional to σ_c^2, and a simplified version of the virial temperature in Equation (2) that is often used is $T_\sigma = \mu m_p \sigma_c^2/k$; T_σ, of course, overestimates the true $\langle T_* \rangle$.

The mass-averaged injection temperature is finally given by

$$\langle T_{\rm inj} \rangle = \langle T_* \rangle + 1.7(f/0.85) \times 10^7 \text{ K}, \quad (3)$$

where, in general, the second term dominates, as is shown in Section 5 below.

2.3. Heating during Infall

In the case of mass losses flowing to the galactic center, the gas can be heated due to infall in the galactic potential and adiabatic compression; this process is sometimes referred to as "gravitational heating." The average change in gravitational energy per unit of gas mass flowing in through the galactic potential down to the galactic center is

$$E^+_{\rm grav} = \frac{1}{M_*} \int_0^\infty 4\pi r^2 \rho_*(r)[\phi(r) - \phi(0)] dr \quad (4)$$

for galaxy mass distributions with a finite value of $\phi(0)$ (see also Ciotti et al. 1991). One can define the temperature equivalent to the energy in Equation (4) as $\langle T^+_{\rm grav} \rangle = 2\mu m_p\, E^+_{\rm grav}/3k$. As $\langle T_* \rangle$, $\langle T^+_{\rm grav} \rangle$ is also $\propto \sigma_c^2$ and increases with larger $\mathcal{R}$ and smaller β, which, for inflowing gas, can be understood as a larger gas heating by compression during infall for a larger dark matter amount or for more concentrated dark matter.

Not all of $E^+_{\rm grav}$ can be available for heating, though. If the inflow remains quasi-hydrostatic, then, according to the virial theorem, the energy radiated away is roughly one-half of the change in the gravitational potential energy, and the part available for the heating of the gas is the remaining half[1] (i.e., $\sim 0.5 E^+_{\rm grav}$). Actually, the energy available for heating will be much less than this. Inflows are caused by the radiative losses produced by the accumulation of stellar mass return, which makes the cooling time less than the galactic age; in the central regions, within a radius of $\sim$1 kpc, the cooling time can be as short as $\lesssim 10^8$ yr, even shorter than the infall time (e.g., Sarazin & White 1988; Pellegrini 2011). In these conditions, the gas departs from a slow inflow, becomes very dense and supersonic close to the center, and cools rapidly down to low temperatures, so that $>0.5 E^+_{\rm grav}$ is radiated away or goes into the kinetic energy of condensations (Sarazin & Ashe 1989). Furthermore, there is a possibility that not all the gas is hot when it reaches the galactic central regions if thermal instabilities develop and produce drop-outs from the flow; if gas cools and condenses out of the flow at large radii, then $E^+_{\rm grav}$ can be much lower than in the definition above, and heating from infall in the gravitational potential is "lost" (Sarazin & Ashe 1989). In conclusion, without precise knowledge of how to compute $E^+_{\rm grav}$ (which depends on the radius at which the injected gas drops below X-ray-emitting temperatures) and about what fraction of $E^+_{\rm grav}$ is radiated or goes into the kinetic energy of the condensations, $\langle T^+_{\rm grav} \rangle$ remains a reference value. A more direct use can instead be made

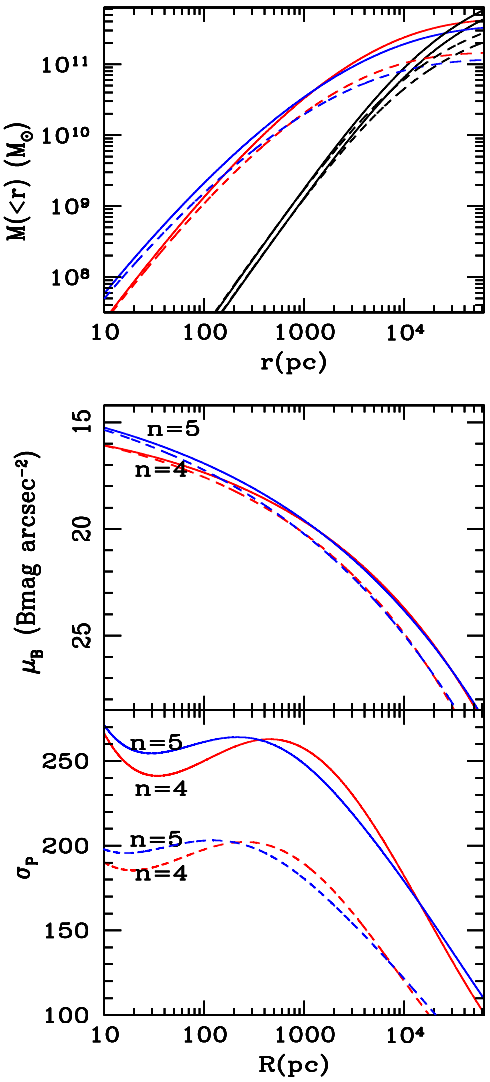

Figure 1. Mass (top), B-band surface brightness (middle), and projected velocity dispersion (bottom) profiles of three-component galaxy models (MBH + stars + dark matter) for two representative ETGs with isotropic orbits and an aperture velocity dispersion within $R_e/8$ of $\sigma_c = 260$ km s^{-1} (solid lines; $L_B = 5 \times 10^{10} L_{B,\odot}$ and $R_e = 6.5$ kpc) and $\sigma_c = 200$ km s^{-1} (dashed lines; $L_B = 2 \times 10^{10} L_{B,\odot}$ and $R_e = 3.6$ kpc). Red lines refer to a stellar Sérsic profile with index $n = 4$ and blue ones to a profile with $n = 5$. The dark halo in the upper panel (black, with the same line type as the corresponding stellar profile) follows the NFW profile, with $\beta = 2$ and $\mathcal{R} = 3$ (for $n = 4$) or $\mathcal{R} = 5$ (for $n = 5$); then, $\mathcal{R}_e = 0.24$ or 0.41, from the Jeans equations (see Section 4). (A color version of this figure is available in the online journal.)

[1] The energy lost in radiation and that converted into heat are actually each equal to $0.5 E^+_{\rm grav}$ for a self-gravitating gas; for gas in an external potential, the result should remain roughly valid (Binney & Tremaine 1987).

of the analogous temperature for escape $\langle T^-_{\rm grav}\rangle$, introduced in Section 3.

2.4. Heating from a Central MBH

Because of the presence of a central MBH in ETGs, another potential source of gas heating could be provided by nuclear accretion. This subject has recently been studied intensely, through both observations and modeling, and it appears that the energy provided by accretion is of the order of that needed to cyclically offset the cooling of the inflowing gas in the central regions of gas-rich ETGs (e.g., Bîrzan et al. 2004; Million et al. 2010; Pellegrini et al. 2011). Therefore, the central MBH is believed to be a heat source that balances the radiative losses of the gas, acting mostly in the central cooling region. In gas-poor ETGs, the nuclear accretion energy is far lower due to the very small mass accretion rate, if present (Pellegrini et al. 2007), and the absorption of the energy output from accretion is likely not efficient. Given the role of the MBH outlined above, possible energy input from the MBH will not be considered as a source of global heating of gas.

3. CONDITIONS FOR ESCAPE

Another characteristic temperature for comparison with observed T values is the temperature with which the gas can escape from the galaxy. Assuming that the flow is stationary and adiabatic, the Bernoulli constant on each streamline along which the gas flows out of the galaxy must be positive. The Bernoulli equation with the minimum energy for escape is written as $H(r)+v^2(r)/2+\phi(r)=0$, where $H=\frac{\gamma}{\gamma-1}\frac{kT}{\mu m_p}=\frac{c_s^2}{\gamma-1}$ is the enthalpy per unit of gas mass, γ is the ratio of specific heats, c_s is the sound velocity, and v is the flow velocity. Integrating over galaxy volume and gas-mass averaging, this condition becomes

$$\int_0^\infty 4\pi r^2\rho_*(r)H(r)dr+\frac{1}{2}\int_0^\infty 4\pi r^2\rho_*(r)v^2(r)dr=M_*E^-_{\rm grav}, \quad (5)$$

where the escape energy

$$E^-_{\rm grav}=-\frac{1}{M_*}\int_0^\infty 4\pi r^2\rho_*(r)\phi(r)dr \quad (6)$$

is the average energy required to remove a unit of gas mass from the galaxy. $E^-_{\rm grav}$ gives a minimum energy requirement, since energy losses from cooling may be present, but these are not important for outflows that typically have a low density (e.g., Section 5.3). The escape temperature equivalent to $E^-_{\rm grav}$ is $\langle T^-_{\rm grav}\rangle=2\mu m_p E^-_{\rm grav}/3k$. The condition for the minimum energy for escape can then be translated into a condition for the injection temperature of the gas $\langle T_{\rm inj}\rangle$ to be larger than $\langle T^-_{\rm grav}\rangle$. In the simple case that $\phi(r)$ is due only to one (stellar) mass component, from $\langle T_*\rangle=2\mu m_p E_{\rm kin}/3kM_*$ and the virial theorem (Section 2), one derives that $\langle T^-_{\rm grav}\rangle=4\langle T_*\rangle$. The estimates of $E^-_{\rm grav}$ in Equation (6) and $\langle T^-_{\rm grav}\rangle$ are calculated below for a general mass model (e.g., made by the superposition of stars and dark matter with different radial distributions). In previous works, the sufficient condition for the existence of a galactic wind was that the injection temperature exceeded an "escape temperature," defined as $2T_\sigma$ (White & Chevalier 1983) or "twice the equivalent dark halo temperature" (Loewenstein & Mathews 1987), and that the radiative cooling time in the central part of the galaxy was longer than the time required to flow out of this region. These conditions are similar to imposing that $\langle T_{\rm inj}\rangle$ exceeds $\langle T^-_{\rm grav}\rangle$, as derived above.

In principle, the gas can escape with different combinations of v and T, and the observed T should be close[2] to that entering H in Equation (5). There are two extreme cases for the value of the flow velocity v with respect to c_s (i.e., to the temperature). One is when the material is brought to infinity, keeping a subsonic velocity, and the minimum energy requirement becomes $H\approx-\phi$; neglecting the kinetic term in Equation (5), one then obtains a characteristic gas-mass-averaged subsonic escape temperature:

$$\langle T^{\rm sub}_{\rm esc}\rangle=\frac{2\mu m_p}{5kM_*}\int_0^\infty 4\pi r^2\rho_*(r)\phi(r)dr=\frac{3}{5}\langle T^-_{\rm grav}\rangle. \quad (7)$$

In the general case, $H\approx-\phi$ gives for T a larger requirement than obtained when v is not neglected; the partition of the gas energy between enthalpy and kinetic energy also can vary with radius within a galaxy. All this means that $\langle T^{\rm sub}_{\rm esc}\rangle$ represents a fiducial upper limit to the observed temperatures of outflowing gas: if the kinetic energy of the flow is important, then the actual gas temperature will be lower (the stronger the outflow, with respect to c_s, the cooler the gas). In the opposite extreme case, in which the temperature's contribution to the gas energy is minor and that of velocity is dominant, the Bernoulli equation reduces to $v^2_{\rm esc}/2+\phi=0$; this gives the usual escape velocity of a unit of mass from a potential well: $v_{\rm esc}(r)=\sqrt{2|\phi(r)|}$.

Finally, $\langle T^-_{\rm grav}\rangle$ and $\langle T^{\rm sub}_{\rm esc}\rangle$ have the same dependence as $\langle T_*\rangle$ on σ_c^2, $\mathcal{R}$, and β. For the representative galaxy mass models used here (Section 4, Figure 2), $E^+_{\rm grav}=(1.7\text{–}2.3)E^-_{\rm grav}$; because $\lesssim 0.5E^+_{\rm grav}$ can be converted into heat, the corresponding temperature gained by infall is $T_{\rm infl}\lesssim\langle T^-_{\rm grav}\rangle$.

4. GALAXY MASS MODELS

In this work, the exact values of $\langle T_*\rangle$, $\langle T^{\rm sub}_{\rm esc}\rangle$, and $\langle T^-_{\rm grav}\rangle$ are calculated as a function of σ_c for a series of representative three-component galaxy mass models, which are made via the superposition of a stellar distribution and a dark matter halo, to which a central MBH is added. The stellar density profile is given by the deprojection of a Sérsic law with index $n=4$ or 5, as appropriate for ETGs of the luminosities considered in this work (e.g., Kormendy et al. 2009). The mass of the MBH is $M_{BH}=10^{-3}M_*$, in agreement with the Magorrian et al. (1998) relation. The dark halo has the Navarro et al. (1997; Navarro–Frenk–White, NFW) profile [$\rho_h\propto 1/(r/r_h)(1+r/r_h)^2$], where r_h is the scale radius, and the profile is truncated at large radii; M_h is the total mass. For each σ_c, the defining parameters of the stellar mass model were chosen according to the observational constraints that L_B must follow the Faber–Jackson relation and that L_B, σ_c, and the effective radius R_e must lie on the fundamental plane of ETGs (e.g., Bernardi et al. 2003). The free parameters defining dark matter were chosen in agreement with the results from dynamical modeling of the observed motions of stars, planetary nebulae, and globular clusters at small and large radii; these indicate that dark matter begins to be dynamically important at 2–3 R_e (e.g., Saglia et al. 1992; Cappellari et al. 2006; Weijmans et al. 2009; Shen & Gebhardt 2010). This requires

[2] For example, one recalls two approximations made here with respect to the case of real ETGs: the total gas profile may be different from that of the stars, and the flow has a time-continuous distributed mass and energy input. The first of these points will be further discussed in Section 5.

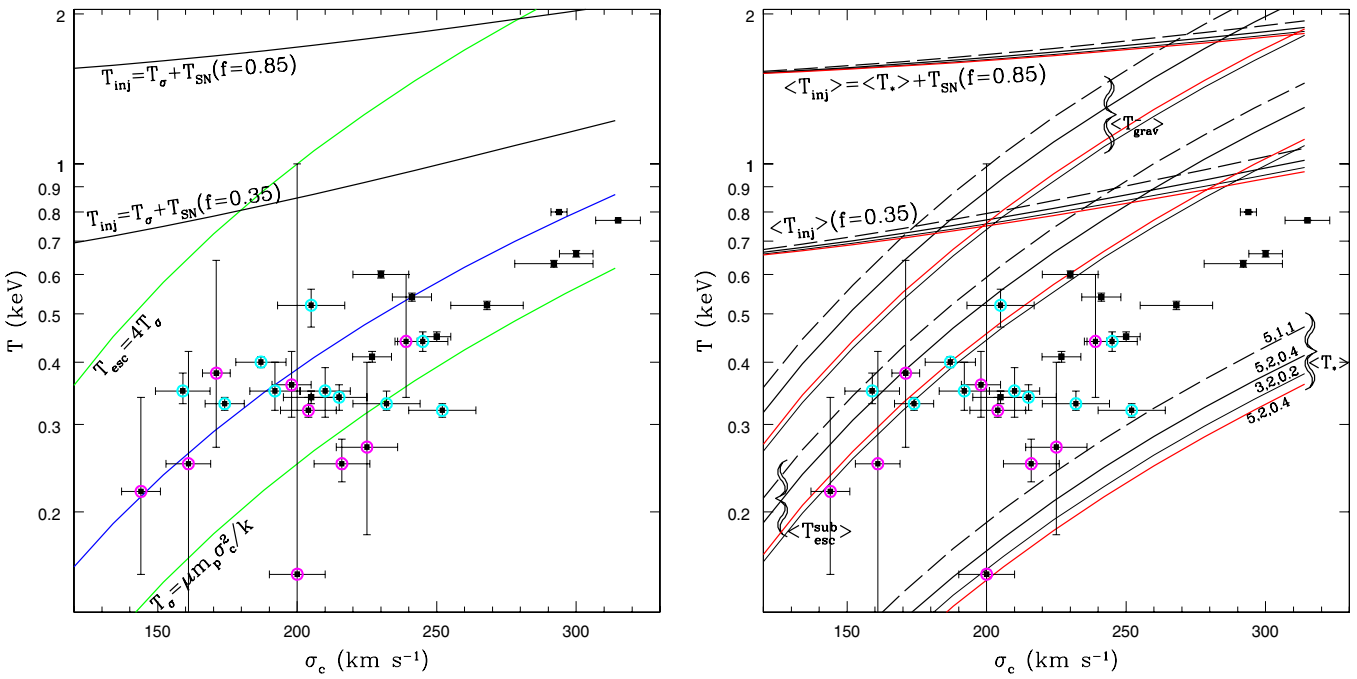

Figure 2. Relationship between the observed gas temperature (from BKF) and σ_c (see Section 5.1). Symbols surrounded by magenta and cyan circles have, respectively, 10^{38} erg s^{-1} $< L_X <$ 1.5×10^{39} erg s^{-1} and 1.5×10^{39} erg s^{-1} $< L_X <$ 1.2×10^{40} erg s^{-1}; all other ETGs have larger L_X. Left panel: in green, T_σ (Section 2) and the simple estimate of $4T_\sigma$ for the escape temperature (Section 3); in blue, the best-fit $\sigma_c \propto T^{0.56\pm0.09}$ found from *ROSAT* data (O'Sullivan et al. 2003); in black, two cases of $T_{\rm inj}$ (Equation (3)), calculated using T_σ. Right panel: (1) $\langle T_* \rangle$ (Equation (2), lowest bundle of lines), calculated for four representative galaxy mass models (made of MBH + stars + dark halo) with a Sérsic index $n = 4$ (black lines) or $n = 5$ (red line) and with the dark matter parameters $\mathcal{R}$, β, $\mathcal{R}_e$ indicated on each curve (Section 4); (2) $\langle T^-_{\rm grav} \rangle$ and $\langle T^{\rm sub}_{\rm esc} \rangle$ (Section 3) for the same mass models adopted for $\langle T_* \rangle$, with the corresponding line type and color; (3) $\langle T_{\rm inj} \rangle$, calculated using $\langle T_* \rangle$, with the corresponding line type and color, and $f = 0.85$ or $f = 0.35$ in Equation (3).

(A color version of this figure is available in the online journal.)

that $\beta = r_h/R_e > 1$ and $\mathcal{R} = M_h/M_* = 3$ or 5 (the latter value corresponds to the baryon-to-total-mass ratio of the *Wilkinson Microwave Anisotropy Probe*; Komatsu et al. 2009). By numerically solving the Jeans equations for the three mass components in the isotropic orbits case (e.g., Binney & Tremaine 1987), these choices produce M_*, M_h, and $\mathcal{R}_e$ (the dark-to-luminous mass ratio within R_e). Reasonable values of $M_*/L_B = (4\text{–}10)\ M_\odot/L_{B,\odot}$ and $\mathcal{R}_e = 0.2\text{–}1.0$ are obtained. The main properties of a few representative mass models are shown in Figure 1.

For a consistent comparison between observed T's and the characteristic temperatures derived for the mass models, the central stellar velocity dispersion σ_c must be the same for observed ETGs and models. Typically, for nearby well-observed ETGs, the value of σ_c is that of the projected and luminosity-weighted average within an aperture of radius $R_e/8$. Therefore, when defining a mass model, the chosen value of σ_c was assigned to this quantity. Finally, streaming motions such as stellar rotation were not considered in these models (possible heating from these motions is discussed by Ciotti & Pellegrini 1996).

5. DISCUSSION

I investigate here the relationship between the observed T's and those expected from the various sources of heating (stellar motions, gravitational potential, SNe Ia) or during the escape of the hot gas. To illustrate this, Figure 2 shows the run with σ_c of the various temperatures defined in Sections 2.2, 2.3, and 3, together with the distribution of the observed T values from BKF (Section 1). For the BKF sample, the value of σ_c is the luminosity-weighted average within $R_e/8$, taken from SAURON studies for 12 ETGs (Kuntschner et al. 2010); for the remaining cases, σ_c is taken from the references in the Hyperleda catalog (see Table 1).

The temperatures defined in Sections 2.2, 2.3, and 3 are mass-weighted averages, which are required when discussing energetic aspects of the gas (e.g., the energy required for escape as measured by $\langle T^-_{\rm grav} \rangle$ compared with the input energy from SNe Ia). When a direct comparison is made with observed T's, it must be noted that the latter coincide with mass-weighted averages only if the entire ISM has one temperature value; if the gas is multi-phase, or its temperature profile has a gradient, a single T value measured from the spectrum of the integrated emission will be close to an emission-weighted average (e.g., Ciotti & Pellegrini 2008; Kim 2011). This means that, since the densest region is the central one, the measured T's tend to be closer to the central values than the mass-weighted ones. The temperature profiles observed with *Chandra* change continuously in shape as the emission-weighted average T decreases from $\lesssim$1 keV to $\sim$0.3 keV: they switch from a flat central profile that increases outside of $\sim 0.5R_e$ to a quasi-isothermal profile to a profile with a negative gradient (Diehl & Statler 2008; Nagino & Matsushita 2009). Therefore, the lowest observed T's, presumably associated with the last category, may be larger than mass-weighted values; intermediate T's may be the closest to mass-weighted averages; and the largest observed T's may be lower than mass-weighted averages. Another aspect to recall is that the temperatures defined in Sections 2.2, 2.3, and 3 refer to a gas distribution with $\rho_{\rm gas} \propto \rho_*$; this is appropriate for continuously injected gas (e.g., for $\langle T_{\rm inj} \rangle$), but it may be less accurate when comparing observed T's with $\langle T^{\rm sub}_{\rm esc} \rangle$ or when

Table 1
Observed Properties of the ETG Sample

Name	kT (keV)	1σ Error	L_X (10^{40} erg s^{-1})	σ_c (km s^{-1})	Ref.
(1)	(2)	(3)	(4)	(5)	(6)
NGC 720	0.54	−0.01; +0.01	5.06	241	Binney et al. (1990)
NGC 821	0.15	−0.05; +0.85	2.13×10^{-3}	200	Kuntschner et al. (2010)
NGC1023	0.32	−0.01; +0.02	6.25×10^{-2}	204	Kuntschner et al. (2010)
NGC1052	0.34	−0.02; +0.02	4.37×10^{-1}	215	Binney et al. (1990)
NGC1316	0.60	−0.01; +0.01	5.35	230	D'Onofrio et al. (1995)
NGC1427	0.38	−0.11; +0.26	5.94×10^{-2}	171	D'Onofrio et al. (1995)
NGC1549	0.35	−0.04; +0.04	3.08×10^{-1}	210	Longo et al. (1994)
NGC2434	0.52	−0.05; +0.04	7.56×10^{-1}	205	Longo et al. (1994)
NGC2768	0.34	−0.01; +0.01	1.26	205	Kuntschner et al. (2010)
NGC3115	0.44	−0.10; +0.16	2.51×10^{-2}	239	Fisher (1997)
NGC3377	0.22	−0.07; +0.12	1.17×10^{-2}	144	Kuntschner et al. (2010)
NGC3379	0.25	−0.02; +0.03	4.69×10^{-2}	216	Kuntschner et al. (2010)
NGC3384	0.25	−0.15; +0.17	3.50×10^{-2}	161	Kuntschner et al. (2010)
NGC3585	0.36	−0.05; +0.06	1.47×10^{-1}	198	Fisher (1997)
NGC3923	0.45	−0.01; +0.01	4.41	250	Pellegrini et al. (1997)
NGC4125	0.41	−0.01; +0.01	3.18	227	Bender et al. (1994)
NGC4261	0.66	−0.01; +0.01	7.02	300	Bender et al. (1994)
NGC4278	0.32	−0.01; +0.01	2.63×10^{-1}	252	Kuntschner et al. (2010)
NGC4365	0.44	−0.02; +0.02	5.12×10^{-1}	245	Bender et al. (1994)
NGC4374	0.63	−0.01; +0.01	5.95	292	Kuntschner et al. (2010)
NGC4382	0.40	−0.01; +0.01	1.19	187	Kuntschner et al. (2010)
NGC4472	0.80	−0.00; +0.00	18.9	294	Bender et al. (1994)
NGC4473	0.35	−0.03; +0.05	1.85×10^{-1}	192	Kuntschner et al. (2010)
NGC4526	0.33	−0.01; +0.02	3.28×10^{-1}	232	Kuntschner et al. (2010)
NGC4552	0.52	−0.01; +0.01	2.31	268	Kuntschner et al. (2010)
NGC4621	0.27	−0.09; +0.13	6.08×10^{-2}	225	Kuntschner et al. (2010)
NGC4649	0.77	−0.00; +0.00	11.7	315	Bender et al. (1994)
NGC4697	0.33	−0.01; +0.01	1.91×10^{-1}	174	Binney et al. (1990)
NGC5866	0.35	−0.02; +0.03	2.42×10^{-1}	159	Fisher (1997)

Notes. Column 1: galaxy name; Columns 2–4: the hot gas temperature, its uncertainty, and the 0.3–8 keV gas luminosity, from BKF; Column 5: the stellar velocity dispersion as the luminosity-weighted average within an aperture of radius $R_e/8$, with its reference in Column 6.

discussing the energetics of the entire gas content of an ETG by means of $\langle T^+_{\rm grav}\rangle$ and $\langle T^-_{\rm grav}\rangle$, since the bulk of the hot ISM may have a different distribution from that of the stars. For example, the observed X-ray brightness profile of gas-rich ETGs was found to follow the optical profile, which was taken as evidence that, roughly, $\rho_{\rm gas} \propto \sqrt{\rho_*}$ (e.g., Sarazin & White 1988; Fabbiano 1989). For gas-poor ETGs hosting galactic winds, modeling shows that the profile $\rho_{\rm gas}(r)$ again will be shallower than $\rho_*(r)$, though not as much as in the previous case (see, e.g., White & Chevalier 1983). If $\rho_{\rm gas}$ has a flatter radial profile than ρ_*, then it is easy to show that its mass-weighted $\langle T^+_{\rm grav}\rangle$ will be larger than that derived using Equation (4), and its mass-weighted $\langle T^-_{\rm grav}\rangle$ and $\langle T^{\rm sub}_{\rm esc}\rangle$ will be lower than derived using Equations (6) and (7). In conclusion, the comparison of observed T's with mass-weighted expectations is the best that can currently be done in a general analysis such as the present work, albeit with the warnings above. Note, however, that all arguments and conclusions below remain valid or are strengthened when taking into account the above considerations about observed T's or about the modifications to $\langle T^+_{\rm grav}\rangle$, $\langle T^-_{\rm grav}\rangle$, and $\langle T^{\rm sub}_{\rm esc}\rangle$.

5.1. Observed and Predicted Temperatures in the $T - \sigma_c$ Plane

In the left panel of Figure 2, the observed T's are compared with approximate estimates of the stellar temperature T_σ, $T_{\rm inj}$, and the escape temperature $4T_\sigma$ (Section 3). The gas luminosity is also indicated with different colors; the L_X values are grouped in three ranges and have a roughly equal number of ETGs in each range. This grouping gives an indication of the gas flow status, based on previous works: a galactic wind leaving the galaxy at supersonic velocity has $L_X < 10^{38}$ erg s^{-1} (e.g., Mathews & Baker 1971; Trinchieri et al. 2008); global subsonic outflows and partial winds can reach $L_X \sim 10^{40}$ erg s^{-1} (Ciotti et al. 1991; Pellegrini & Ciotti 1998); and a central inflow becomes increasingly more important in ETGs of increasingly large L_X. Magenta ETGs (10^{38} erg s^{-1} $< L_X < 1.5\times10^{39}$ erg s^{-1}) should then host winds, subsonic outflows, and partial winds with a very small inflowing region of radius <100 pc; cyan ETGs (1.5×10^{39} erg s^{-1} $< L_X < 1.2 \times 10^{40}$ erg s^{-1}) should host subsonic outflows and partial winds with an increasingly large inflowing region (of radius up to a few hundred pc); and black ETGs are hot gas-rich and mostly inflowing.[3] The best fit found for X-ray bright ETGs is also shown in the left panel (O'Sullivan et al. 2003) and gives a good representation of the distribution of observed T's down to a range of low temperatures and gas contents never before explored. The slope of the fit ($T \propto \sigma_c^{1.79}$)

[3] In the X-ray faintest ETGs, the gas emission L_X is ∼(1–2) times the integrated emission from the population of weak, unresolved stellar sources (Section 1), generally referred to as AB + CVs. BKF derived an AB + CV emission model by jointly fitting the M31 and M32 spectra, and then tested how the measurement of the gas properties may be affected by the adopted AB + CV model (their Section 3.1). By fitting with different AB + CV models, all within the uncertainties in the adopted one, the measured T values changed only negligibly for the six lowest L_X ETGs of their sample; a systematic uncertainty of 10%–20% was found for the gas flux (but was much lower for the X-ray brighter ETGs).

and that of the $T_\sigma \propto \sigma_c^2$ relation are similar, with the fit being shallower; this could be because not all heating sources depend on σ_c^2—see, e.g., the important SNe Ia contribution in $T_{\rm inj}$, which produces a much flatter run of $T_{\rm inj}$ with σ_c (Figure 2). The fit was mostly based on gas-rich ETGs, whose T's show a trend with σ_c closer to that of T_σ (an aspect further addressed in Sections 5.2 and 6), while gas-poor ETGs depart most from it, since their T's change little for largely varying σ_c (as found by BKF; see Section 5.4).

The right panel of Figure 2 shows the stellar temperature $\langle T_* \rangle$, injection temperature $\langle T_{\rm inj} \rangle$, escape temperature $\langle T^-_{\rm grav} \rangle$, and the characteristic temperature for the slowly outflowing gas $\langle T^{\rm sub}_{\rm esc} \rangle$, calculated for a set of representative galaxy mass models (Section 4). At any fixed σ_c and Sérsic index n, $\langle T_* \rangle$, $\langle T^-_{\rm grav} \rangle$, and $\langle T^{\rm sub}_{\rm esc} \rangle$ are larger at larger galaxy masses ($\mathcal{R}$) and mass concentrations (smaller β).[4] The dashed lines represent a reasonable upper limit to the values of each characteristic temperature, since they correspond to the most massive model ETGs with the most concentrated dark matter allowed for by recent studies (Section 4). The $\langle T^-_{\rm grav} \rangle$ curves lie below the simple approximation of the escape temperature given by $4T_\sigma$; $\langle T^-_{\rm grav} \rangle = 4.8 \langle T_* \rangle$ for $\mathcal{R} = 3$, and $\simeq 5.2 \langle T_* \rangle$ for the three cases with $\mathcal{R} = 5$.

As expected, all $\langle T_* \rangle$ curves lie below T_σ, which overestimates the kinetic energy associated with the stellar random motions (Section 2.2). Note that, according to the virial theorem, $\langle T_* \rangle$ is independent of orbital anisotropy, which just redistributes the stellar heating differently within a galaxy; the presence of ordered rotation in stellar motions instead requires a more careful consideration. For any fixed galaxy mass model, this rotation would leave the total stellar heating unchanged or lower it, depending on whether the entire stellar streaming motion or just a fraction of it is converted into heat (Ciotti & Pellegrini 1996). In the worst case that the stellar rotational motion is not thermalized at all, and the galaxy is a flat isotropic rotator, $\langle T_* \rangle$ in Figure 2 should be an overestimate of ∼30% of the temperature corresponding to stellar heating (Ciotti & Pellegrini 1996); the possible reduction of $\langle T_* \rangle$ should be lower than this, because the massive ETGs in Figure 2 are less flattened and more pressure-supported systems (e.g., Emsellem et al. 2011).

All observed T's are located above $\langle T_* \rangle$; thus, additional heating with respect to the thermalization of stellar kinetic energy is needed, as noticed previously using T_σ (e.g., Davis & White 1996; BKF). The gas can retain the memory of its injection temperature and have additional infall heating, as examined in Sections 5.2 and 5.3.

Finally, the values of $\langle T_{\rm inj} \rangle$ for $f = 0.85$ are by far the largest temperatures in Figure 2, larger than $\langle T^-_{\rm grav} \rangle$ up to $\sigma_c \sim 250$ km s^{-1}; therefore, SNe Ia should cause the escape of gas from all ETGs up to this σ_c, since the gas at every time is injected with an energy larger than required to leave the galaxy potential. This expectation is fulfilled by all ETGs with $\sigma_c \lesssim 200$ km s^{-1}: their X-ray properties (a low L_X and T's on the order of $\langle T^{\rm sub}_{\rm esc} \rangle$) agree well with what is expected if outflows are important in them. This result has been suggested previously based on the low observed L_X; now, for the first time, it can be confirmed based on the observed T values. At $\sigma_c > 200$ km s^{-1}, instead, ETGs may have L_X far larger than expected for outflows (black symbols), and most ETGs where likely outflows are important (magenta or cyan symbols) have T's much lower than $\langle T^{\rm sub}_{\rm esc} \rangle$; these findings are discussed in Section 5.4.

[4] All other things being equal, these temperatures are also larger at smaller n values, due to the galaxy becoming more massive to reproduce the same σ_c, since the stellar mass profile is less steep (e.g., Figure 1).

5.2. Gravitational Heating in Gas-rich ETGs

I examine here the possibility that the additional heating with respect to the thermalization of the stellar kinetic energy is provided by infall heating and SNe Ia. Davis & White (1996) assumed that the hot gas is flowing in all ETGs and suggested that the observed temperatures are larger than T_σ because the luminous parts of ETGs are embedded in dark matter halos that are dynamically hotter than the stars; i.e., a form of "gravitational potential" way of heating the gas was invoked. This form can consist of an effect of the dark halo on stellar motions, which are then thermalized, or directly on the gas during infall (e.g., via $E^+_{\rm grav}$). The first possibility is excluded by the $\langle T_* \rangle$ curves in Figure 2 that are always lower than T_σ and that, through the Jeans equations, include the effect of a massive dark halo, chosen to be consistent with the current knowledge of the ETGs' structure. In the second possibility, heating from gas infall, $E^+_{\rm grav}$ is potentially an important source of heating that increases with the amount and concentration of dark matter. This can be judged from Figure 2 after considering that $\langle T^-_{\rm grav} \rangle \sim 5 \langle T_* \rangle$ and that the temperature possibly attainable from infall was estimated to be $T_{\rm infl} \lesssim \langle T^-_{\rm grav} \rangle$ (see the end of Section 3). Note that $T_{\rm infl}$ (if it behaves like $\langle T^+_{\rm grav} \rangle$) could be $\propto \sigma_c^2$, a trend close to that shown by the T's of gas-rich ETGs (BKF; see also Section 6).

Inflowing ETGs can also benefit from the SNe Ia energy input; for the unit mass of injected gas, this is written as $E^{\rm tot}_{\rm SN} = R_{\rm SN} E_{\rm SN} / \dot{M}_*$. Both $E^+_{\rm grav}$ and $E^{\rm tot}_{\rm SN}$ contribute to the required additional thermal energy with respect to that gained from the stellar random motions, i.e., to $\Delta E_{\rm th} = 3k(T - \langle T_* \rangle)/2\mu m_p$. $E^+_{\rm grav}$ and $E^{\rm tot}_{\rm SN}$ in large part can be radiated in gas-rich ETGs, but they seem to far exceed the required $\Delta E_{\rm th}$. For example, for the highest L_X of Figure 2, $\Delta E_{\rm th} \sim (1\text{–}2) \times 10^{48}$ erg $M_\odot^{-1}$ (i.e., ∼ 0.2–0.4 keV), when adopting an average galaxy mass model such as that represented by the thick black line in Figure 2. The energy spent in radiation can be estimated, in a stationary situation, as $L_X / \dot{M}_*$ (per unit of injected gas mass); using the L_X from BKF and deriving $\dot{M}_*$ as in Section 2.1 for the same distances in BKF and galactic B-magnitudes given by Hyperleda, for gas-rich ETGs one finds that $L_X / \dot{M}_*$ ranges between $(0.5\text{–}3.4) \times 10^{48}$ erg $M_\odot^{-1}$. The energy available is far larger than the sum of $\Delta E_{\rm th}$ and $L_X / \dot{M}_*$: $E^{\rm tot}_{\rm SN} = 7.3 \times 10^{48} (f/0.85)$ erg $M_\odot^{-1}$, and $0.5 E^+_{\rm grav}$ ranges from 4×10^{48} erg $M_\odot^{-1}$ ($\sigma_c \sim 220$ km s^{-1}) to 8×10^{48} erg $M_\odot^{-1}$ ($\sigma_c \sim 300$ km s^{-1}) in the mass model with the thick black line in Figure 2. These results are detailed in Figure 3, where the values of $\Delta E_{\rm th}$ and $L_X / \dot{M}_*$ for each galaxy are shown, together with various combinations of $E^+_{\rm grav}$ and $E^{\rm tot}_{\rm SN}$. In conclusion, additional energy input for the gas, to account for the observed T's of gas-rich ETGs, seems to be available in a sufficient amount, even if f were to be <0.85.

5.3. Outflows and SNe Ia Heating

The gas is not mostly inflowing in all ETGs, while it is hotter than $\langle T_* \rangle$ in all of them. When in outflow, the radiative losses are far smaller, but energy is spent in extracting the gas from the galaxy and giving it a bulk velocity. I discuss here the possibility that heating from the SNe Ia energy input accounts for the

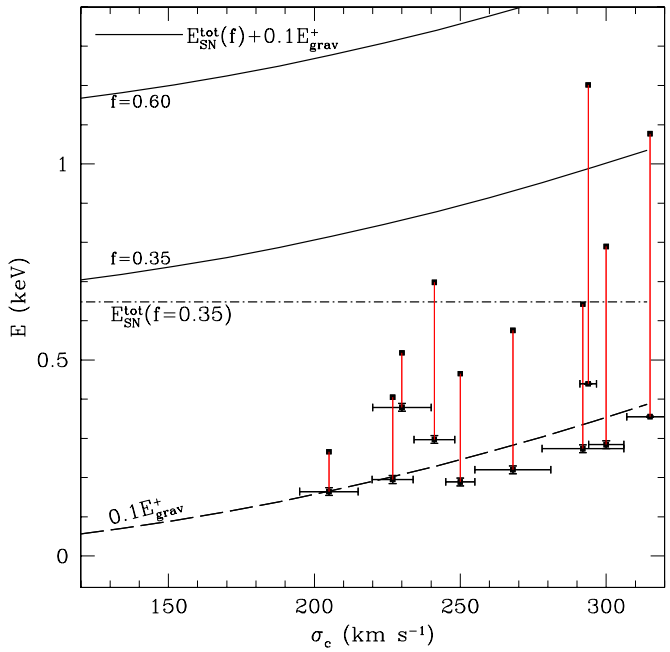

Figure 3. Run with σ_c of the energies provided by SNe Ia (E^{tot}_{SN}) and gas infall (E^{+}_{grav}); points with error bars show, for the ETGs with the largest L_X in Figure 2, the additional thermal energy (ΔE_{th}), with respect to that gained from the thermalization of stellar random motions, required to explain the observed T's (see Section 5.2). These energies (E^{tot}_{SN}, E^{+}_{grav}, and ΔE_{th}), which are defined per unit of mass in the text, have been multiplied by $2\mu m_p/3$ to obtain their temperature equivalents in keV plotted here. Solid lines show the sum of the energies provided by the SNe Ia and infall for two cases of f and for E^{+}_{grav} rescaled by a factor of 0.1, calculated for the galaxy mass model described by the thick black line in Figure 2 (right panel). The dashed line gives the value of $0.1E^{+}_{grav}$ for reference, and the dot-dashed line represents the value of E^{tot}_{SN} for $f = 0.35$. The points with error bars are obtained by subtracting from the observed kT the value of $k\langle T_*\rangle$ corresponding to its σ_c for the mass model adopted for E^{+}_{grav}; each point is linked by a red line to a point that includes the energy spent in radiation observed for that ETG (i.e., the upper point measures $\Delta E_{th} + L_X/\dot{M}_*$). See Section 5.2 for more details.

(A color version of this figure is available in the online journal.)

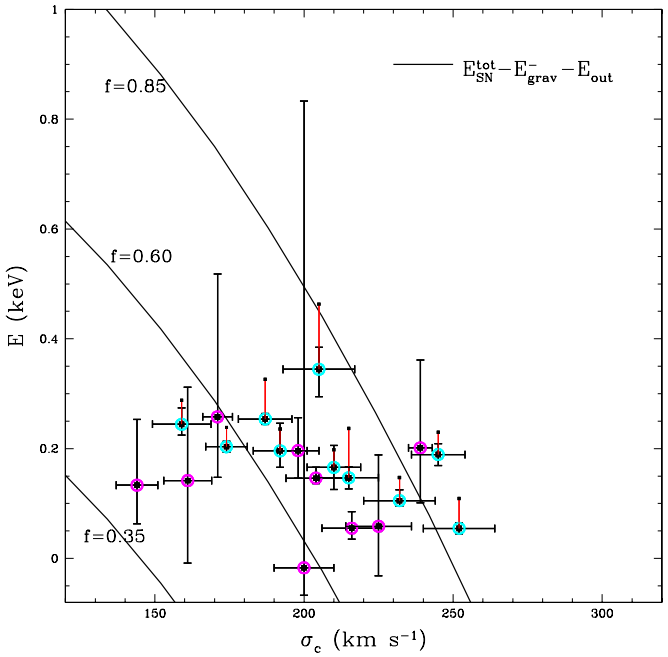

Figure 4. Run with σ_c of the energy provided by SNe Ia (E^{tot}_{SN}, for three cases of f) after subtraction of the energy needed for the removal of the gas from the galaxy (E^{-}_{grav}) and for escape (E_{out}) at an average $v_{out} = c_s$(0.3 keV); all energies were computed as in Figure 3. The adopted galaxy mass model corresponds to the thick black line in Figure 2 (right panel). Points with error bars show the additional thermal energy required to explain the observed T's, calculated as in Figure 3, for ETGs with low/medium L_X in Figure 2. For the cyan ETGs, a red line connects each point with the value that includes the radiated energy, as in Figure 3; the red lines of the magenta ETGs, whose L_X values are the lowest, would be included within the colored circle if shown. See Section 5.3 for more details.

(A color version of this figure is available in the online journal.)

observed ΔE_{th} of ETGs where outflows are likely important (those with low/medium L_X—the magenta and cyan symbols in Figure 2).

I assume that the SNe Ia energy is used for the uplift of gas and the kinetic energy with which gas escapes from the galaxy, and, neglecting radiative losses, that the remaining part can account for the observed ΔE_{th}. Then the energy balance per unit mass of injected gas is $E^{tot}_{SN} = E^{-}_{grav} + E_{out} + \Delta E_{th}$, where ΔE_{th} is the same as in Section 5.2 and $E_{out} = v^2_{out}/2$ is the mass-averaged kinetic energy of the escaping material per unit of gas mass. Figure 4 shows ΔE_{th} derived from this balance, with $v_{out} = c_s$, and c_s calculated for $\gamma = 5/3$ and $kT = 0.3$ keV, a temperature on the order of that observed for ETGs that are likely in outflow (Figure 2). Adopting $v_{out} \sim c_s$ (independent of σ_c) produces E_{out} at the upper end of those expected,[5] and then the estimate of ΔE_{th} may be biased low. With $v_{out} \sim c_s$, E_{out} is just $\sim 0.1(f/0.85)E^{tot}_{SN}$. The energy needed for gas extraction, E^{-}_{grav}, for the same galaxy mass model used in Section 5.2, varies instead from $\sim 1/3(f/0.85)E^{tot}_{SN}$ for $\sigma_c = 150$ km s^{-1} to $\sim E^{tot}_{SN}$ for $\sigma_c = 250$ km s^{-1}; this explains the strong dependence of the predicted ΔE_{th} on σ_c in Figure 4. It is clear from this figure that, for $f = 0.85$, SNe Ia can account for the required heating in all ETGs with low/medium L_X; for $f = 0.35$, however, the temperature increase would fall short of that required for all ETGs. In Figure 4, the energy losses due to radiation are also shown; their small size supports the hypothesis that in most cases they do not significantly affect the energy budget of the gas.

Given the flat distribution of the observed points in Figure 4 and the steep behavior of the curves predicting ΔE_{th}, the value of f required to account for the observed ΔE_{th} increases with σ_c. In particular, the value $f \sim 0.85$ that is required at high σ_c would produce an expected ΔE_{th} at low σ_c that is larger than observed. A possible solution could reside in the efficiency of the SNe Ia energy-mixing process. In massive, gas-rich ETGs, SNe Ia bubbles should disrupt and share their energy with the local gas within $\sim 3 \times 10^6$ yr (Mathews 1990); for a Milky Way–size bulge in a global wind, however, three-dimensional hydrodynamical simulations of discrete heating from SNe Ia suggest a non-uniform thermalization of SNe Ia energy, with overheated gas from an SNe Ia explosion at the bulge center that is advected outward, carrying a large fraction of SNe Ia energy with it (Tang et al. 2009). For subsonic outflows, the mixing is expected to be more local and more complete (Lu & Wang 2011). The magenta and cyan ETGs in Figure 4 have gas densities and luminosities larger than those considered by Tang et al. (2009); however, if a discrete heating effect were still present at $\sigma_c < 200$ km s^{-1}, it could qualitatively explain a

[5] For example, in a wind solution, the terminal (i.e., the largest) velocity of the flow is roughly the central sound speed (White & Chevalier 1983); moreover, in this solution, the gas is likely to be already too "fast" with respect to that of most magenta ETGs in Figure 2, due to their L_X (e.g., Trinchieri et al. 2008).

lower f for these galaxies. It is also possible that $\langle T_* \rangle$ has been overestimated (and then the observed $\Delta E_{\rm th}$ underestimated) at low σ_c if these ETGs are less pressure-supported systems (e.g., Emsellem et al. 2011) and stellar rotational streaming is not entirely thermalized (Section 5.1). Another possible explanation could be that ETGs with $\sigma_c > 200$ km s^{-1} are less outflow-dominated than those at lower σ_c (though this is not supported solely based on L_X, since magenta ETGs are found over the entire σ_c range in Figure 4), so that their $E^-_{\rm grav}$ would be lower than assumed by the curves in Figure 4, and more SNe Ia energy would be available for heating. In this way, f could have a value <0.85 and possibly be similar for all ETGs.

Finally, a comparison of Figures 3 and 4 shows that the average $\Delta E_{\rm th}$ is slightly larger for the X-ray brightest ETGs (for which it ranges between 0.1 and 0.5 keV) than for the X-ray faintest ones (0–0.3 keV); moreover, while the $\Delta E_{\rm th}$ in Figure 3 can be explained even with $f < 0.85$, it is required that $f \sim 0.85$ for the X-ray faintest ETGs with the largest σ_c in Figure 4. Both facts are the consequence of the large fraction of SNe Ia energy input that is used in gas extraction where outflows dominate, while all SNe Ia energy remains within the galaxies where inflow dominates.

In conclusion, even for ETGs with low/medium L_X, a fundamental X-ray property such as T can be accounted for by simple arguments, simply based on realistic galaxy mass models and reasonable SNe Ia heating capabilities. There may, however, be more energy available for the gas in ETGs with $\sigma_c < 200$ km s^{-1} than can be accounted for by the present simple scenario.

5.4. The Temperature and Gas Flow Status in ETGs of Intermediate Mass

The observed X-ray properties (low L_X and $T \sim \langle T^{\rm sub}_{\rm esc} \rangle$) and the energy budget of the gas (e.g., $\langle T^-_{\rm grav} \rangle$ versus $\langle T_{\rm inj} \rangle$) for ETGs with $\sigma_c \lesssim 200$ km s^{-1} are all consistent with the expectations for outflows; the large L_X and $\langle T^-_{\rm grav} \rangle$ larger than $\langle T_{\rm inj} \rangle$ of ETGs with $\sigma_c > 250$ km s^{-1} agree with gas that is mostly inflowing. For $200 < \sigma_c$(km s^{-1}) < 250, however, ETGs show very different L_X and T, whose values seem unrelated to $\langle T^{\rm sub}_{\rm esc} \rangle$ and to the relative size of $\langle T^-_{\rm grav} \rangle$ and $\langle T_{\rm inj} \rangle$ (Figure 2). For example, for $f = 0.85$, $\langle T_{\rm inj} \rangle$ exceeds $\langle T^-_{\rm grav} \rangle$, but most T values lie well below $\langle T^{\rm sub}_{\rm esc} \rangle$, and even high L_X values (incompatible with outflows) are common. One primary explanation could be that $f < 0.85$; for example, for $f = 0.35$, $\langle T_{\rm inj} \rangle$ becomes lower than $\langle T^-_{\rm grav} \rangle$ at $\sigma_c \sim 180$ km s^{-1} (Figure 2). Four ETGs with $\sigma_c > 200$ km s^{-1} and very low L_X (Figure 2, magenta symbols), though, require that f be > 0.35 for them, and then that f vary from galaxy to galaxy, or that their gas be removed by other processes such as an active galactic nucleus outburst (e.g., Machacek et al. 2006; Ciotti et al. 2010), a merging, or an interaction (Read & Ponman 1998; Sansom et al. 2006; Brassington et al. 2007). An event similar to the latter two is unlikely in the recent past for three of these ETGs (NGC1023, NGC3115, NGC3379), which are very regular in their stellar morphological and kinematic properties, but is possible in the other ETG (NGC4621) that hosts a counter-rotating core (Wernli et al. 2002).

A second explanation could be that $\langle T_{\rm inj} \rangle$ exceeds $\langle T^-_{\rm grav} \rangle$ only in the present epoch: while $\langle T_* \rangle$ and $\langle T^-_{\rm grav} \rangle$ are independent of time, $T_{\rm SN}$ may have been lower in the past (Equation (1)), to the point that $\langle T_{\rm inj} \rangle$ may have been lower than $\langle T^-_{\rm grav} \rangle$ for more ETGs than in Figure 2 (which represents a snapshot of the present epoch). The gas then could have accumulated and radiative losses become important, even for the gas injected in later epochs. In fact, the population synthesis models of Section 2 predict that $\dot{M}_*$ was larger at early times (e.g., by $\sim$6 times at an age of 3 Gyr); to keep $T_{\rm SN}$ high in the past, then, from Equation (1), $\dot{M}_{\rm SN}$ must decrease with time t at a rate similar to or steeper than that of the stellar mass losses ($\dot{M}_* \propto t^{-1.3}$; Ciotti et al. 1991). Recent observational estimates indicate instead an SNe Ia rate that decays close to t^{-1} (Maoz et al. 2011; Sharon et al. 2010); thus, $T_{\rm SN}$ and $\langle T_{\rm inj} \rangle$ should be increasing with time, reaching the values of Figure 2 in the present epoch. Then a "cooling effect of the past" would explain a moderate or high L_X even where $\langle T_{\rm inj} \rangle$ exceeds $\langle T^-_{\rm grav} \rangle$ in Figure 2.

Both explanations, $f < 0.85$ and/or a lower $\langle T_{\rm inj} \rangle$ in the past, can account for the lack of a widespread presence of outflows for $200 < \sigma_c$(km s^{-1}) < 250. Both, though, require a mechanism different from the SNe Ia energy input to cause degassing in some low L_X ETGs in the same σ_c range.

Another possibility is that partial winds become common for $\sigma_c > 200$ km s^{-1}: these ETGs host an inner inflow and an outer outflow (e.g., MacDonald & Bailey 1981), with variations in galactic structure causing different sizes of the inflowing regions and different L_X (Pellegrini & Ciotti 1998). This possibility holds even for $f = 0.85$ and for both kinds of time evolution of $\langle T_{\rm inj} \rangle$; in fact, if the flow is decoupled, ETGs may host a central inflow even if $\langle T_{\rm inj} \rangle$ is larger than $\langle T^-_{\rm grav} \rangle$. Similarly, the observed T's can be lower than $\langle T^{\rm sub}_{\rm esc} \rangle$ in ETGs where the outflow is only external; in this case, the observed T's may be lowered also by radiative losses in the central inflowing region.

6. THE TEMPERATURE OF INFLOWS AND OUTFLOWS

In Figure 2, the hottest gas is in ETGs with the highest L_X, and the coolest gas is in ETGs with the lowest L_X (as also found by BKF). This feature is also present in the $L_X - \sigma_c$ relation, where ETGs with $kT > 0.4$ keV have the brightest X-rays (with one exception) and those with $kT < 0.3$ keV have the faintest X-rays (BKF). All this may seem contrary to the simple expectations that hotter gas is needed for escape and that the hotter the gas, the stronger the outflow and the lower the gas content. We re-examine this point below, first across the entire σ_c range and then at fixed σ_c values.

A proper consideration of whether outflowing ETGs possess hotter or colder gas than inflowing ones requires that all T's be rescaled by a temperature equivalent to the depth of the potential where the gas resides (e.g., by T_σ). Is there a trend in the distance of the observed T's from $\langle T^{\rm sub}_{\rm esc} \rangle$ or $\langle T_* \rangle$? This is examined in Figure 5, where temperatures are rescaled by T_σ and the σ_c^2 dependence of all curves in Figure 2 is removed. Figure 5 shows that for $\sigma_c < 200$ km s^{-1} the observed points reach $\langle T^{\rm sub}_{\rm esc} \rangle / T_\sigma$, a result similar to that in Figure 2, and that they fall below it with increasing σ_c (with a transition region of large dispersion in T/T_σ). Therefore, ETGs with $\sigma_c < 200$ km s^{-1} are indeed the hottest relative to the virial temperature; since in these ETGs outflows are important (Section 5.1), the flow is relatively hotter in outflows, and T increases from outflows to inflows only in an absolute sense. The T's of the X-ray brightest ETGs should show a dependence on σ_c^2 if the gravitational heating of the gas dominates SNe Ia heating, and then they should lie within a horizontal zone in Figure 5. The observed distribution does not disagree with this kind of dependence, but more cases are needed to firmly establish its presence; such a dependence is not expected, though, since the SNe Ia heating should easily dominate the gravitational heating (Section 5.2).

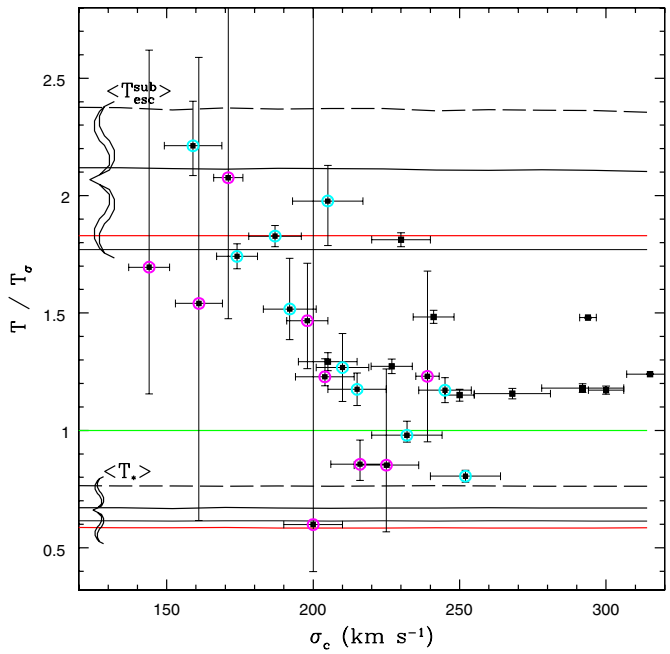

Figure 5. Same as Figure 2 (right panel), with temperature values rescaled by T_σ.

(A color version of this figure is available in the online journal.)

Finally, I compare the T's at similar σ_c in the most populated region of Figure 5 for $200 < \sigma_c(\mathrm{km\ s^{-1}}) < 250$. Here, the variation of T/T_σ is the largest and is covered by ETGs of all X-ray emission levels; the X-ray brightest ETGs have $T/T_\sigma > 1.1$, while the lowest T/T_σ values belong to the X-ray fainter ETGs. For example, two of the three lowest T/T_σ values in the figure (those of NGC3379 and NGC4621) belong to the X-ray faintest group. While heating sources seem abundant in gas-rich ETGs, accounting for their T's (see, e.g., Figure 3 and the additional possibility of MBH heating; Section 2.4), even after taking into account their radiative losses, this result remains more difficult to explain for ETGs of low/medium L_X, and may require ad hoc solutions. It may be another representation of what is mentioned in Section 5.3: that $\Delta E_{\rm th}$ can be larger for the X-ray brightest ETGs than for the X-ray faintest ETGs, due to the different employment of SNe Ia input energy; or it could be that $f < 0.85$ in these ETGs, so that SNe Ia cannot make their gases hotter than this (Figure 4). Moreover their galaxy structures may be very different from an average one, so that dividing all T's for the same T_σ produces a biased view; or the evolutionary history of the gas may have been peculiar. Certainly, this trend needs further investigation and, if confirmed, will provide the basis for further theoretical work.

7. CONCLUSIONS

This work focused on the origin of the hot gas temperatures recently derived for a sample of ETGs observed with *Chandra*, down to galaxy masses and X-ray luminosities smaller than ever before. A few characteristic mass-weighted average temperatures were defined for a gas distribution $\rho_{\rm gas}(r) \propto \rho_*(r)$, such as for the gas shed by stars: the virial temperature $\langle T_*\rangle$; the injection temperature $\langle T_{\rm inj}\rangle$, that is the sum of $\langle T_*\rangle$ and of a temperature equivalent to the SNe Ia kinetic energy input (with a factor f allowing for its uncertain thermalization); the escape temperature $\langle T^-_{\rm grav}\rangle$, defined as the temperature equivalent to the energy required for escape from the gravitational potential; a fiducial value for the temperature of escaping gas, evaluated on a streamline of very subsonic velocity ($\langle T^{\rm sub}_{\rm esc}\rangle = 0.6\langle T^-_{\rm grav}\rangle$); and, finally, the temperature equivalent to the energy liberated by the inflow of gas to the galactic center, $\langle T^+_{\rm grav}\rangle$. These temperatures were then calculated for a set of representative galaxy mass models, made by the superposition of a central MBH and of a stellar and a dark mass density distribution, with parameters constrained by the fundamental scaling laws of ETGs and recent observational findings. The main properties of the characteristic temperatures are the following.

1. All temperatures scale as σ_c^2 (except for $\langle T_{\rm inj}\rangle$) and increase for larger and/or more concentrated mass content. For the adopted set of representative galaxy mass models, $\langle T_*\rangle$ is lower than T_σ (by $\sim$0.1–0.2 keV), $\langle T^-_{\rm grav}\rangle \approx 5\langle T_*\rangle$, and $\langle T^+_{\rm grav}\rangle \approx 2\langle T^-_{\rm grav}\rangle$; the temperature that can be produced by infall heating, though, will be much lower than $\langle T^-_{\rm grav}\rangle$, due to energy losses in radiation, the kinetic energy of mass condensations, and mass drop-outs from the flow.
2. $\langle T_{\rm inj}\rangle$ is by far the largest of the characteristic temperatures due to the important SNe Ia contribution (independent of σ_c); for $f = 0.85$, it is larger than the minimum injection temperature for global escape up to $\sigma_c \sim 250$ km s^{-1}.

The comparison of the characteristic temperatures with those observed, in the $T - \sigma_c$ plane, shows the following.

1. The best-fit $T - \sigma_c$ relation previously found for X-ray bright ETGs reproduces the average trend of the observed T down to low temperatures and low L_X. ETGs with low/medium L_X show the largest departures from this fit, which can be explained by the variety of gas-flow phases possible in them (winds, subsonic outflows, partial winds), where the main input energies (from SNe Ia and gas infall) are used in different ways.
2. All observed T's are larger than $\langle T_*\rangle$; the additional heating of gas $\Delta E_{\rm th}$, with respect to that provided by the thermalization of stellar motions, is $\Delta E_{\rm th} \approx$ 0–0.3 keV for the X-ray faintest ETGs and $\Delta E_{\rm th} \approx$ 0.1–0.5 keV for the X-ray brightest ETGs (for a representative galaxy mass model).
3. In a stationary situation, $\Delta E_{\rm th}$ of the X-ray brightest ETGs can be accounted for by the energy input of SNe Ia and gas infall, even if they are much reduced with respect to standard assumptions (i.e., f can be <0.85). The gravitational heating produces a $T \propto \sigma_c^2$ trend that may be present in the X-ray brightest ETGs; the SNe Ia heating, though, is expected to be dominant.
4. $\Delta E_{\rm th}$ can be provided by SNe Ia in X-ray fainter ETGs, where outflows are important; most of the SNe Ia energy is needed for gas extraction, and less for the kinetic energy of the escape. The value of f to account for the observed $\Delta E_{\rm th}$ increases with σ_c, until the entire SNe Ia energy ($f \approx 0.85$) is required at the highest σ_c. With this f, though, at low σ_c the observed $\Delta E_{\rm th}$ is lower than expected. Possible solutions require a different efficiency of the SNe Ia energy-mixing process, or an overestimate of $\langle T_*\rangle$ at low σ_c if these ETGs are less pressure-supported systems, or a more complex flow status than in the simple scheme adopted.
5. At low $\sigma_c \lesssim 200$ km s^{-1}, $\langle T_{\rm inj}\rangle$ is larger than $\langle T^-_{\rm grav}\rangle$, the L_X values are low, and the T's are on the order of $\langle T^{\rm sub}_{\rm esc}\rangle$: all this agrees well with what is expected for outflows. At high $\sigma_c > 250$ km s^{-1}, $\langle T_{\rm inj}\rangle$ is lower than $\langle T^-_{\rm grav}\rangle$, and the high L_X and T values can be explained by the mostly inflowing gas. For $200 < \sigma_c(\mathrm{km\ s^{-1}}) < 250$, instead, there is a large

variation in L_X and T. Possible explanations could be that the SNe Ia energy input varies from galaxy to galaxy; and/or that $\langle T_{\rm inj}\rangle$ was lower in the past due to the different time evolutions of the mass loss and the SNe Ia rate; or that partial winds become common, with the flow status less related to the values of $\langle T_{\rm inj}\rangle$, $\langle T^{-}_{\rm grav}\rangle$, and $\langle T^{\rm sub}_{\rm esc}\rangle$.

6. When measured relative to the depth of the potential well, the observed temperatures T/T_σ are larger for $\sigma_c < 200$ km s^{-1} (outflows) and lower for $\sigma_c > 250$ km s^{-1} (inflows). The observed T's then increase from outflows to inflows only in an absolute sense, and the gas is relatively hotter in outflows. In the intermediate region of $200 < \sigma_c({\rm km\ s^{-1}}) < 250$, lower L_X values tend to correspond to lower T and T/T_σ values, which requires ad hoc explanations and deserves further observational and theoretical investigation.

I thank Luca Ciotti for helpful discussions, and Dong-Woo Kim and the referee for useful comments.

REFERENCES

Athey, A., Bregman, J., Bregman, J., Temi, P., & Sauvage, M. 2002, ApJ, 571, 272
Auger, M. W., et al. 2010, ApJ, 724, 511
Bender, R., Saglia, R. P., & Gerhard, O. E. 1994, MNRAS, 269, 785
Bernardi, M., et al. 2003, AJ, 125, 1866
Binney, J., Davies, R. L., & Illingworth, G. D. 1990, ApJ, 361, 78
Binney, J., & Tremaine, S. 1987, Galactic Dynamics (Princeton, NJ: Princeton Univ. Press)
Bîrzan, L., Rafferty, D. A., McNamara, B. R., Wise, M. W., & Nulsen, P. E. J. 2004, ApJ, 607, 800
Boroson, B., Kim, D. W., & Fabbiano, G. 2011, ApJ, 729, 12
Brassington, N. J., Ponman, T. J., & Read, A. M. 2007, MNRAS, 377, 1439
Brown, B. A., & Bregman, J. N. 2000, ApJ, 539, 592
Cappellari, M., et al. 2006, MNRAS, 366, 1126
Cappellaro, E., Evans, R., & Turatto, M. 1999, A&A, 351, 459
Chevalier, R. A. 1974, ApJ, 188, 501
Ciotti, L., D'Ercole, A., Pellegrini, S., & Renzini, A. 1991, ApJ, 376, 380
Ciotti, L., Ostriker, J. P., & Proga, D. 2010, ApJ, 717, 708
Ciotti, L., & Pellegrini, S. 1992, MNRAS, 255, 561
Ciotti, L., & Pellegrini, S. 1996, MNRAS, 279, 240
Ciotti, L., & Pellegrini, S. 2008, MNRAS, 387, 902
David, L. P., Forman, W., & Jones, C. 1990, ApJ, 359, 29
David, L. P., Jones, C., Forman, W., Vargas, I. M., & Nulsen, P. 2006, ApJ, 653, 207
Davis, D. S., & White, R. E., III. 1996, ApJ, 470, L35
Diehl, S., & Statler, T. S. 2007, ApJ, 668, 150
Diehl, S., & Statler, T. S. 2008, ApJ, 687, 986
D'Onofrio, M., Zaggia, S., Longo, G., Caon, N., & Capaccioli, M. 1995, A&A, 296, 319
Emsellem, E., et al. 2011, MNRAS, 414, 888
Eskridge, P. B., Fabbiano, G., & Kim, D.-W. 1995, ApJS, 97, 141
Fabbiano, G. 1989, ARA&A, 27, 87
Fabbiano, G. 2006, ARA&A, 44, 323
Fisher, D. 1997, AJ, 113, 950
Gallo, E., Treu, T., Marshall, P. J., Woo, J.-H., Leipski, C., & Antonucci, R. 2010, ApJ, 714, 25
Gisler, G. R. 1976, A&A, 51, 137
Kim, D. W. 2011, in Hot Interstellar Matter in Elliptical Galaxies, ed. D. W. Kim & S. Pellegrini, Astrophysics and Space Science Library, Vol. 378 (Heidelberg: Springer)
Komatsu, E., et al. 2009, ApJS, 180, 330
Kormendy, J., Fisher, D. B., Cornell, M. E., & Bender, R. 2009, ApJS, 182, 216
Kuntschner, H., et al. 2010, MNRAS, 408, 97
Larson, R. B. 1974, MNRAS, 166, 585
Li, W., et al. 2011, MNRAS, 412, 1473
Loewenstein, M., & Mathews, W. G. 1987, ApJ, 319, 614
Longo, G., Zaggia, S., Busarello, G., & Richter, G. 1994, A&AS, 105, 433
Lu, Z., & Wang, Q. D. 2011, MNRAS, 413, 347
MacDonald, J., & Bailey, M. E. 1981, MNRAS, 197, 995
Machacek, M., Nulsen, P. E. J., Jones, C., & Forman, W. R. 2006, ApJ, 648, 947
Magorrian, J., et al. 1998, AJ, 115, 2285
Maoz, D., Mannucci, F., Li, W., Filippenko, A. V., Della Valle, M., & Panagia, N. 2011, MNRAS, 412, 1508
Maraston, C. 2005, MNRAS, 362, 799
Mathews, W. G. 1990, ApJ, 354, 468
Mathews, W. G., & Baker, J. C. 1971, ApJ, 170, 241
Memola, E., Trinchieri, G., Wolter, A., Focardi, P., & Kelm, B. 2009, A&A, 497, 359
Million, E. T., et al. 2010, MNRAS, 407, 2046
Nagino, R., & Matsushita, K. 2009, A&A, 501, 157
Napolitano, N. R., et al. 2010, MNRAS, 411, 2035
Navarro, J. F., Frenk, C. S., & White, S. D. M. 1997, ApJ, 490, 493
O'Sullivan, E., Forbes, D. A., & Ponman, T. J. 2001, MNRAS, 328, 461
O'Sullivan, E., Ponman, T. J., & Collins, R. S. 2003, MNRAS, 340, 1375
Parriott, J. R., & Bregman, J. N. 2008, ApJ, 681, 1215
Pellegrini, S. 2010, ApJ, 717, 640
Pellegrini, S. 2011, in Hot Interstellar Matter in Elliptical Galaxies, ed. D. W. Kim & S. Pellegrini, Astrophysics and Space Science Library, Vol. 378 (Heidelberg: Springer)
Pellegrini, S., Baldi, A., Kim, D. W., Fabbiano, G., Soria, R., Siemiginowska, A., & Elvis, M. 2007, ApJ, 667, 731
Pellegrini, S., & Ciotti, L. 1998, A&A, 333, 433
Pellegrini, S., Ciotti, L., & Ostriker, J. P. 2011, ApJ, submitted (arXiv:1107.3675)
Pellegrini, S., & Fabbiano, G. 1994, ApJ, 429, 105
Pellegrini, S., Held, E., & Ciotti, L. 1997, MNRAS, 288, 1
Read, A. M., & Ponman, T. J. 1998, MNRAS, 297, 143
Revnivtsev, M., Churazov, E., Sazonov, S., Forman, W., & Jones, C. 2008, A&A, 490, 37
Saglia, R. P., Bertin, G., & Stiavelli, M. 1992, ApJ, 384, 433
Sansom, A. E., O'Sullivan, E., Forbes, D. A., Proctor, R. N., & Davis, D. S. 2006, MNRAS, 370, 1541
Sarazin, C. L., & Ashe, G. A. 1989, ApJ, 345, 22
Sarazin, C. L., & White, R. E., III. 1988, ApJ, 331, 102
Sharon, K., et al. 2010, ApJ, 718, 876
Shen, J., & Gebhardt, K. 2010, ApJ, 711, 484
Sun, M., Jones, C., Forman, W., Vikhlinin, A., Donahue, M., & Voit, G. M. 2007, ApJ, 657, 197
Tang, S., & Wang, Q. D. 2005, ApJ, 628, 205
Tang, S., Wang, Q. D., Mac Low, M., & Joung, M. R. 2009, MNRAS, 398, 1468
Trinchieri, G., et al. 2008, ApJ, 688, 1000
Weijmans, A. M., et al. 2009, MNRAS, 398, 561
Wernli, F., Emsellem, E., & Cpoin, Y. 2002, A&A, 396, 73
White, R. E., III, & Chevalier, R. 1983, ApJ, 275, 69
White, R. E., III, & Sarazin, C. L. 1991, ApJ, 367, 476